ELSEVIER

Sedimentary Geology 153 (2002) 23–41

Sedimentary Geology

www.elsevier.com/locate/sedgeo

The middle Pleistocene Merced-2 and -3 sequences from Ocean Beach, San Francisco

R.M. Carter [a,*], S.T. Abbott [b], I.J. Graham [c], T.R. Naish [c], P.R. Gammon [d]

[a] *Marine Geophysical Laboratory, James Cook University, 4811 Townsville, Qld, Australia*
[b] *School of Resource Science, Southern Cross University, Lismore, Australia*
[c] *Institute of Geological and Nuclear Sciences, Lower Hutt, New Zealand*
[d] *Department of Geology and Geophysics, University of Adelaide, Adelaide, Australia*

Accepted 23 January 2002

Abstract

The Merced Formation comprises a 2-km-thick shallow marine and non-marine succession that was deposited in a small transtensional basin along the San Andreas Fault during the late Pliocene to middle Pleistocene. The sediments dip between 10° and 80° to the northeast, and are locally disrupted by small faults. During tilting, the beds have been rotated into subparallelism with the San Andreas Fault zone, splays of which bound the outcrop belt of Merced sediments to both the southwest and northeast. The Merced Formation contains more than 20 transgressive–regressive sedimentary rhythms (cyclothems, or sequences) that are generally between 40 and 120 m thick, and which were deposited mostly during interglacial time, under the influence of rising, highstand and early falling sea levels. Sequences Merced-2 [units M1–N of Soc. Econ. Paleontol. Mineral., Field Guidebook 3 (1984) 1] and Merced-3 (units O–P), though in fault contact, comprise typical Plio-Pleistocene shallow water cyclothems. The Merced-2 Sequence is 22+ m thick, and comprises a sandy and shelly transgressive systems tract, including a basal Type A shellbed, an in situ Type B mid-cycle shellbed, and a highstand systems tract of massive siltstone. The Merced-3 Sequence is 47 m thick, and comprises a basal compound shellbed, a thin highstand systems tract siltstone, and a sand-rich regressive systems tract. The RST comprises distal shoreface sands with an abundant in situ molluscan fauna, and upper shoreface and back-beach trough cross-bedded sands and pebbly sands. The top of the Merced-3 cycle comprises a beach sand capped by a palaeosol and lignite (the "Beetle Bed"), which together mark the subaerial exposure of the site during the ensuing glacial sea-level lowstand. Analysis of ^{10}Be across the Merced-3 Sequence shows major peaks, indicative of sedimentation starvation, in the basal transgressive systems tract shellbed and in the capping lignite of the Beetle Bed. Smaller ^{10}Be peaks are associated with a shellbed that is inferred to represent winnowing at the foot of the shoreface, and with a minor exposure surface that delimits a small paracycle in the top of the sequence. Otherwise, ^{10}Be abundances decline regularly across the Merced-3 Sequence, consistent with an increasing sedimentation rate as shoreface progradation, and regression, progressed. The character of cycles Merced-2 and Merced-3 respectively resembles the Seafield and Rangitikei sequence motifs described from similar Plio-Pleistocene sediments in New Zealand. The cycles are of mid-Pleistocene age, and were probably deposited during interglacial oxygen isotope stages 21 and 19, respectively.

Keywords: Middle Pleistocene; Merced Formation; Cyclothems

* Corresponding author. Tel.: +61-77-81-4536; fax: +61-77-251-501.
E-mail address: bob.carter@jcu.edu.au (R.M. Carter).

0037-0738/02/$ - see front matter © 2002 Elsevier Science B.V. All rights reserved.
PII: S0037-0738(02)00099-4

1. Introduction

The Merced Formation outcrops as a coastal strip between Fort Funston and Mussel Rock, on the Pacific coast 15–20 km south of the tip of San Francisco peninsula (Fig. 1). The outcrop comprises a homoclinal sequence that is bounded to the southwest by the San Andreas Fault (Clifton et al., 1988). Dips are between 60° and 80° in the lower part of the section, lessening to 10°–20° near Fort Funston at the north end. The sediments are dominantly unconsolidated sands and muds with intervals of consolidated siltstone, an unstable mix that results in severe landsliding along the coastal cliffs. Rapid tectonic uplift and tilting has caused significant deformation of the sediments, which exhibit many minor faults, shear zones and incipient cleavages. This combination of tectonic deformation and pervasive landsliding poses a significant challenge to reconstructing a detailed stratigraphic record.

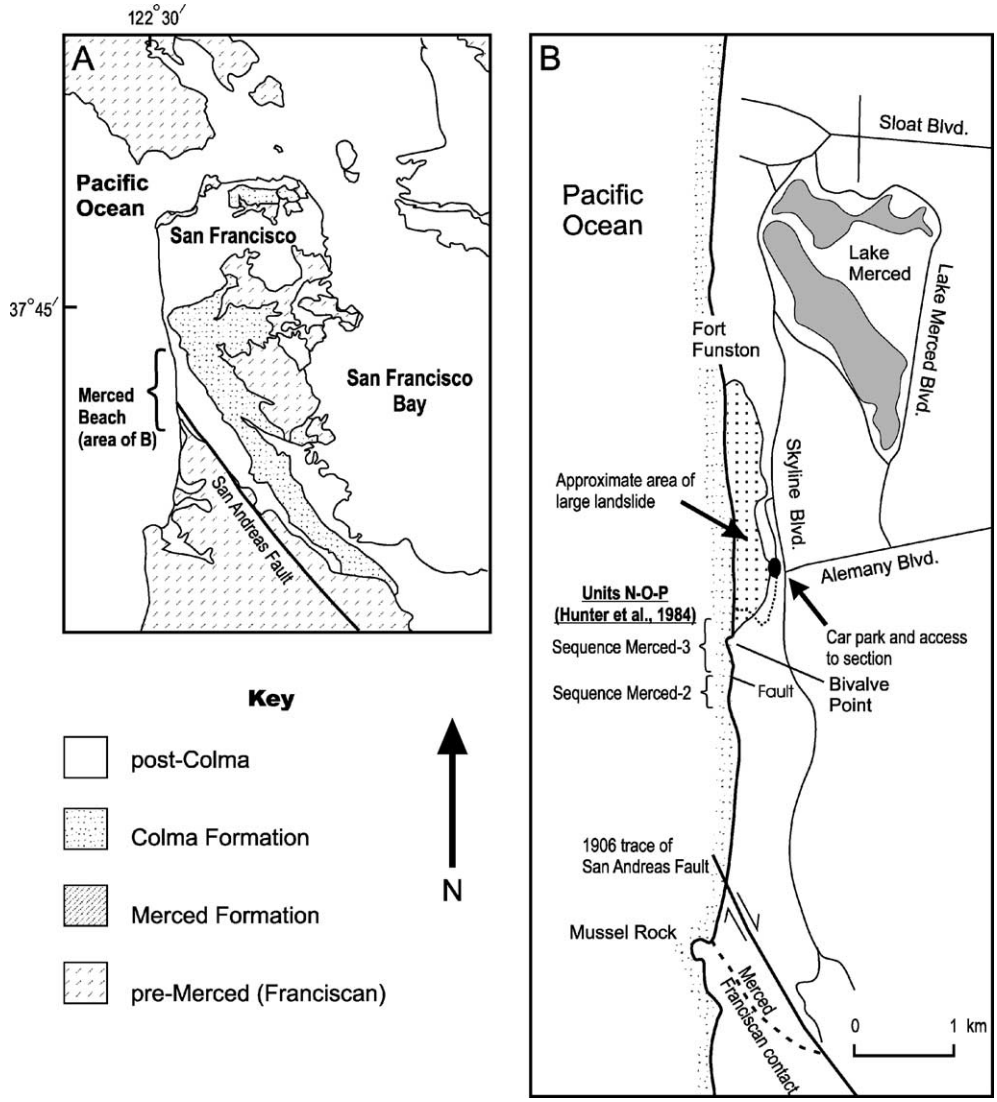

Fig. 1. Locality map for the outcrop occurrence of the Merced-2 and Merced-3 sequences, Ocean Beach, San Francisco (after Hunter et al., 1984).

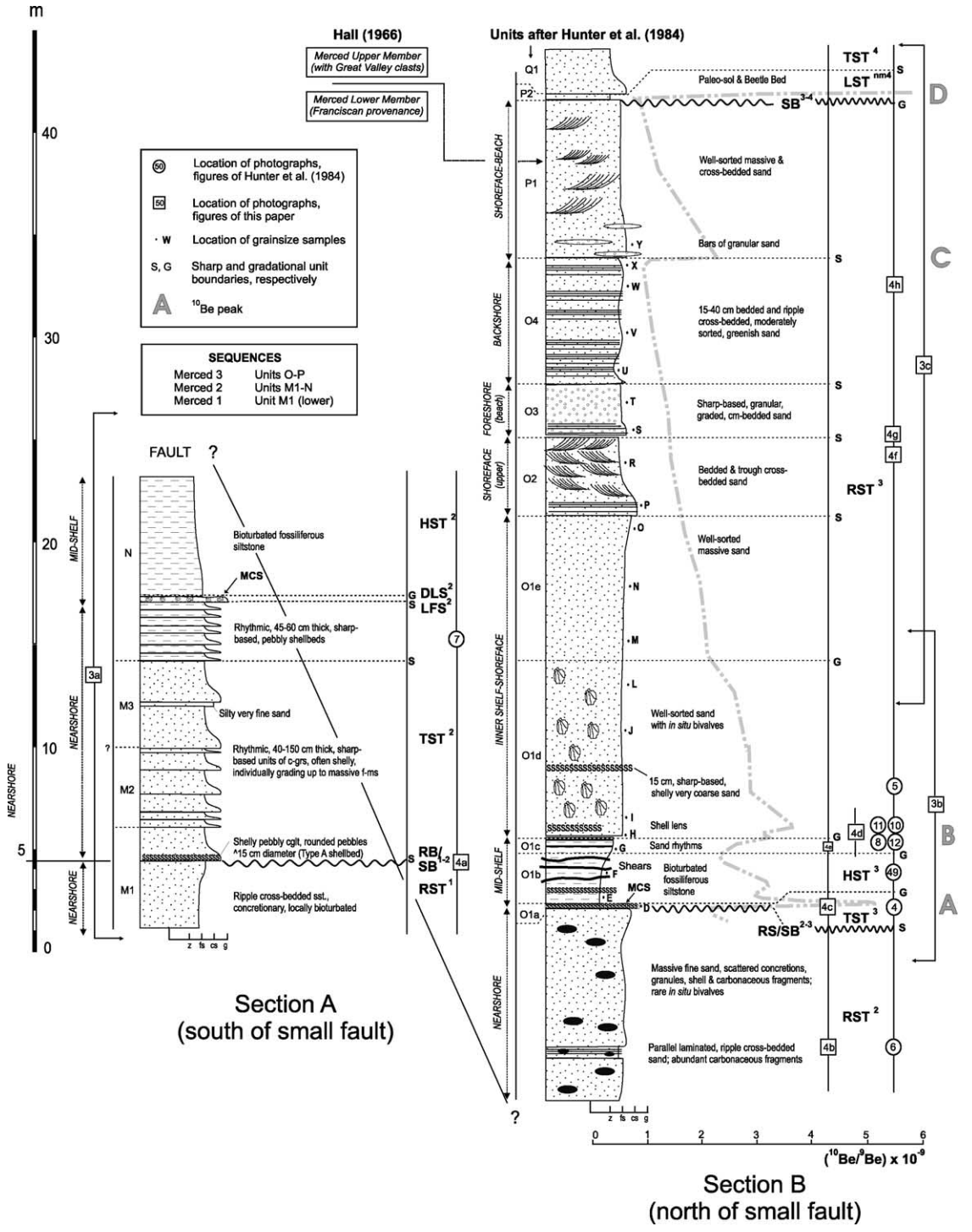

Fig. 2. Measured section of the Merced-2 and Merced-3 sequences at Ocean Beach. Stratigraphic and shellbed terminology after Abbott and Carter (1994) and Naish and Kamp (1997).

Clifton et al. (1988) and Clifton (1989) have shown that the outcropping section of the Merced Formation is 1.75 km thick, and comprises a succession of sedimentary cycles. A typical cycle is 40–120 m thick, and comprises a sharp, erosional contact at the base, a basal pebbly shellbed, a lower interval of shallow

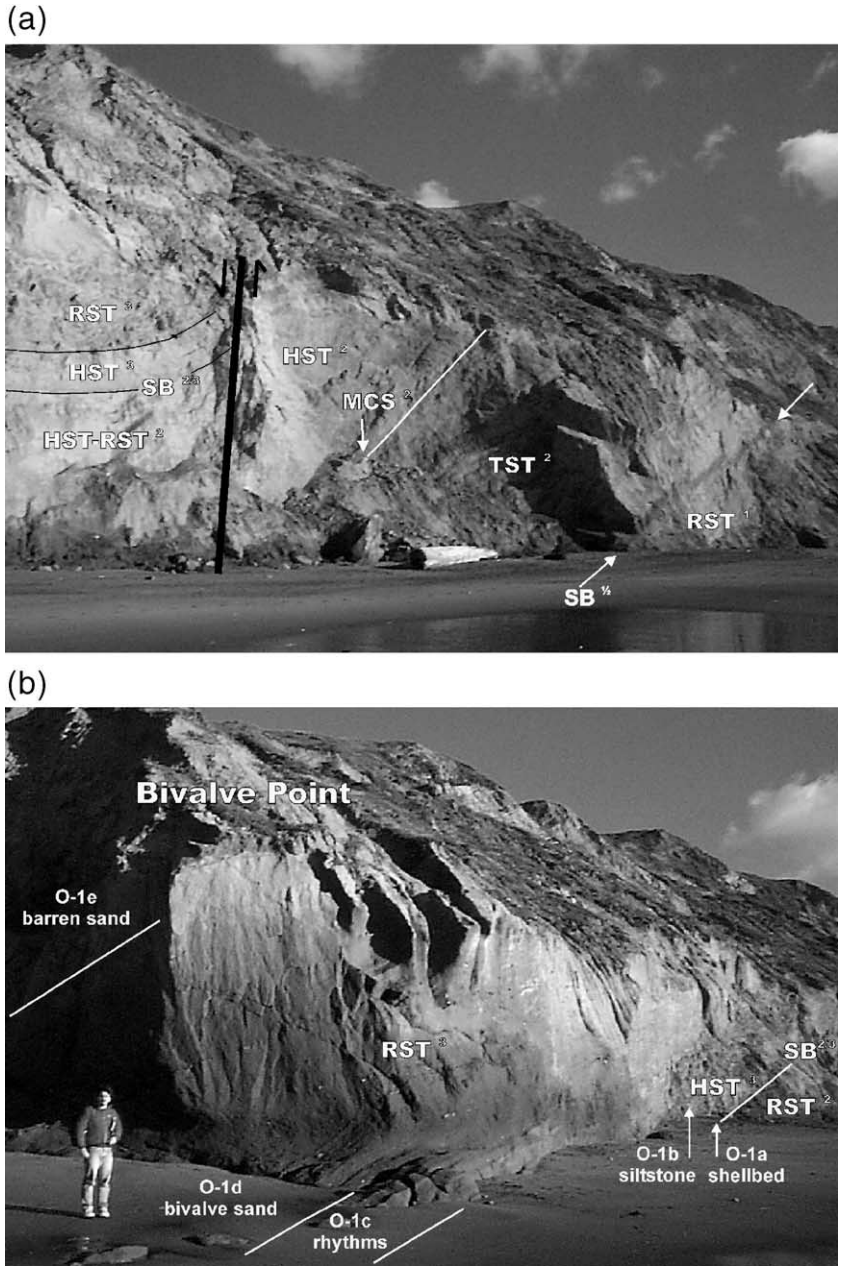

Fig. 3. Outcrop views of the Merced-2 and Merced-3 sequences, Ocean Beach. (a) View towards the southeast of the basal part of the Merced-2 Sequence, and its juxtaposition across a small fault with the upper part of the Merced-2 and basal Merced-3 sequences. Location, south of Bivalve Point. (b) View towards the southeast of the basal part of the Merced-3 Sequence. Location, at Bivalve Point. (c) View towards the south of the middle and upper parts of the Merced-3 Sequence. Location, at and immediately north of Bivalve Point.

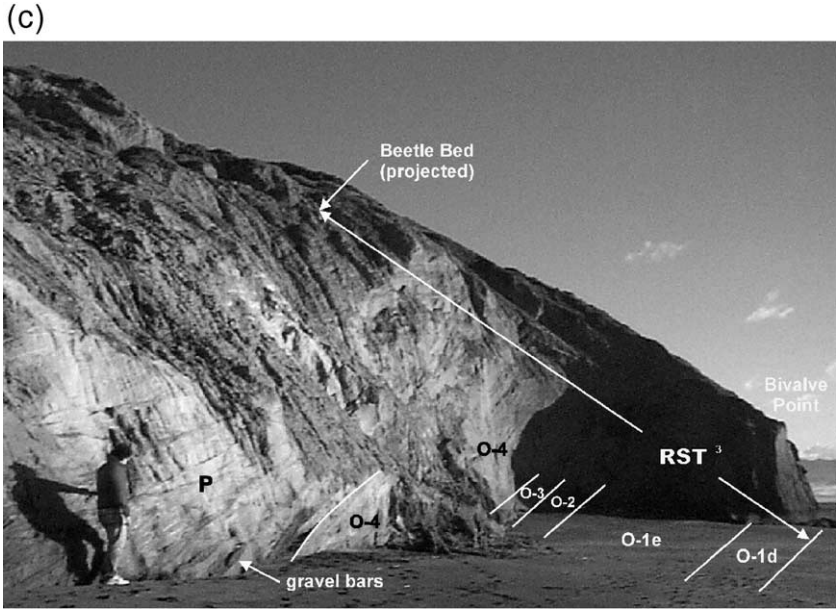

Fig. 3 (*continued*).

marine sands, a middle interval of deeper water siltstones with a shelf molluscan fauna, and an upper interval of shallow marine sands. The cycles become sandier towards the top of the section, where shallow marine, estuarine and non-marine sands of regressive character dominate the cycles (Clifton and Leithold, 1991). Clifton et al. (1988) distinguished more than 20 such sedimentary rhythms, which represent cyclothems or sequences deposited at least partly under the control of Plio-Pleistocene glacio-eustasy. Their recognition of cyclicity was based on the careful description of repetitive changes in sedimentary facies, and a comparison between these facies and their likely modern equivalents. In this study, we have remeasured one small part of the Merced succession, and interpreted its cyclicity in terms of high-resolution sequence stratigraphy.

Though semicontinuous along Ocean Beach, significant parts of the Merced Formation outcrop are obscured by slumping from higher in the cliffs. We have therefore concentrated our analysis on that part of the section that contains sedimentary units M–P of Hunter et al. (1984) and Clifton et al. (1988), within which we recognize three stratigraphic sequences, Merced-1, Merced-2 and Merced-3. The section is often well exposed, particularly after winter storms, and is of generally easy access. For access, vehicles can be parked adjacent to the riding stables just north of the junction of Allemany and Skyline Boulevards, from where a path leads around the south end of a large slump and down to the beach (Fig. 1).

We use the conventional abbreviations TST, MCS, HST and RST for stratigraphic intervals that we infer to represent a transgressive systems tract, mid-cycle shellbed, highstand systems tract, or regressive systems tract, respectively. LST^{nm} refers to non-marine sediments that were deposited landward of the lowstand systems tract shoreline during periods of glaciation. SB, RS, LFS and DLS (e.g. Fig. 2) refer to the four master surfaces that occur within a typical sequence, namely the sequence boundary, ravinement surface, local flooding surface and downlap surface, respectively (cf. Carter, 1998; Carter et al., 1998). Commonly, shoreface erosion of a sediment-starved seabed results in the RS becoming superposed upon the SB during sea-level rise and transgression, and we use the terminology SB/RS for the resulting composite surface. With the addition of a numeric superscript, these abbreviations are also used to refer to systems tracts or surfaces that are specific to a particular sequence (e.g. RST^3 represents the regressive systems tract of sequence 3). We also follow Abbott and Carter (1994)

in recognizing two important types of shellbed within the Merced succession. *Type A shellbeds*, which most often occur immediately above sequence-bounding ravinement surfaces, are characterised by broken and eroded shells of shallow water mollusca intermixed with sandy, well-rounded pebble conglomerate (cf. Chiocci and Clifton, 1991) of inferred TST origin. In contrast, *Type B shellbeds* contain generally deeper water shelf molluscan species (including some in situ double-valved bivalves) set in a muddy sand matrix, and correspond to MCS. Other autocyclic shellbeds can of course occur within shallow marine sequences. A critical part of the recognition of sequence-determining basal TST and MCS shellbeds, therefore, is the correct identification of their respective lower bounding surfaces as significant RS or LFS diastems, together with the overall nature of the facies packages that the shellbeds punctuate.

Hunter et al. (1984, Fig. 2) depicted the sedimentary section across their units M–P as continuous. Though our remeasured section (Fig. 2) matches their earlier observations in most features, storms during the autumn and early winter of 1998 caused fresh erosion of the cliff face and exposed, perhaps for the first time, a fault that truncates the top of unit N (Fig. 3a). The inaccessibility of parts of the cliff, and pervasive slumping, prevented us from measuring the throw of this fault directly. However, comparison with the many other small faults that occur across the section (e.g. Clifton et al., 1988, Fig. 6.4) suggests that the throw is unlikely to be more than 5–15 m. Our remeasurement of this part of the section (Fig. 2) therefore recognizes two main sequence cycles, Merced-2 (units M1–N of Hunter et al., 1984, occurring south of the fault; Fig. 3a), and Merced-3 (units O–P of Hunter et al., 1984, occurring north of the fault; Fig. 3c). The fault apparently does not alter the basic stratigraphy, and acts only to offset a small (and so far immeasurable) portion of unit N, that is, the fault is probably located entirely within the upper HST–RST part of the Merced-2 cycle.

Marine macrofossils are common in the Merced Formation, particularly in shelf siltstone and lower shoreface sand facies. They comprise principally molluscan and echinoderm species that are still living, and are thus of use for palaeoecological determinations but have little value for age determination. Many of the molluscan macrofossils are also fragile, and therefore difficult to extract and identify at species level. Other means of age determination are also sparse. Clifton et al. (1988) report that palaeomagnetic determinations are not possible because of the occurrence of sediment remagnetization. The major age control on the sequence, therefore, is provided by the Rockland tephra that occurs within the top of unit S (Hunter et al., 1984, Fig. 3), two cycles above the Merced-3 Sequence. The established fission track age of 400 ka for this tephra (Sarna-Wojcicki et al., 1985; Meyer et al., 1991) has recently been revised, and $^{40}Ar/^{39}Ar$ dating now indicates a best age of 614 ka (Lanphere et al., 1999, 2000). Using the redated Rockland tephra for guidance, the Merced-3 Sequence was deposited about 800 ka, that is, probably corresponds to interglacial oxygen isotope stage 19 or 21.

2. Sequence Merced-2

Those parts of units M–N of Hunter et al. (1984, Fig. 2) that we include in the Merced-2 Sequence, and that occur to the south of the fault, are 22+ m thick. Hunter et al. (1984, p. 20) reported that "a distinctive gravel 30 cm thick lies in the upper part of unit M1". Large bio-erosional structures at the base of this gravel appear to be produced by large bivalves, some of which (*Tresus*?) are preserved in living position. We take this pebbly shellbed to mark the base of the Merced-2 Sequence, and its base as a marine ravinement surface which has been superposed upon, and has eroded, a former subaerial unconformity.

The superposition of similar facies below (inner shelf, RST) and above (inner shelf, TST) a sequence boundary, as in this case (Fig. 2), is not an uncommon occurrence in successions that represent basinal nearshore (at highstand) conditions. Indeed, such occurrences are a primary cause of ambiguity as to the correct late-TST, HST or early-RST interpretation of many Holocene shoreface successions (cf. Larcombe and Carter, 1998). In older examples, however, identification is normally aided by the fact that the RST caps a shoaling–sanding upward succession, and the TST starts a deepening–fining upward succession.

2.1. Transgressive systems tract

The Merced-2 cycle commences with a 45-cm-thick pebbly shellbed (intra-M1) resting on a sharp, un-

dulating surface of erosion with up to 30 cm of pebble and shell-filled incision (Figs. 2 and 3a). Similar shellbed bases have been illustrated in Chiocci and Clifton (1991). The underlying bioturbated, bedded and cross-bedded concretionary sandstone was interpreted as an inner shelf deposit by Hunter et al. (1984, p. 20), and we treat it as part of the RST of the Merced-1 Sequence. The basal Merced-2 shellbed contains worn and broken molluscan shells in a matrix of poorly sorted, pebbly, medium sand, with occasional pebbles up to 15 cm in diameter (Fig. 4a). Bivalve shells occur as single valves that are aligned with the bedding and dominantly preserved convex-side-up. The shellbed is clearly current deposited, and has a similar appearance to the Type A shellbeds that characterise the TST of mid-Pleistocene shellbeds in New Zealand (Abbott and Carter, 1994). The basal shellbed is overlain by several rhythms of well-sorted, massive, sandstone, in which the sharp base of each rhythm is followed by a thin bed of coarser grained granular or pebbly sand.

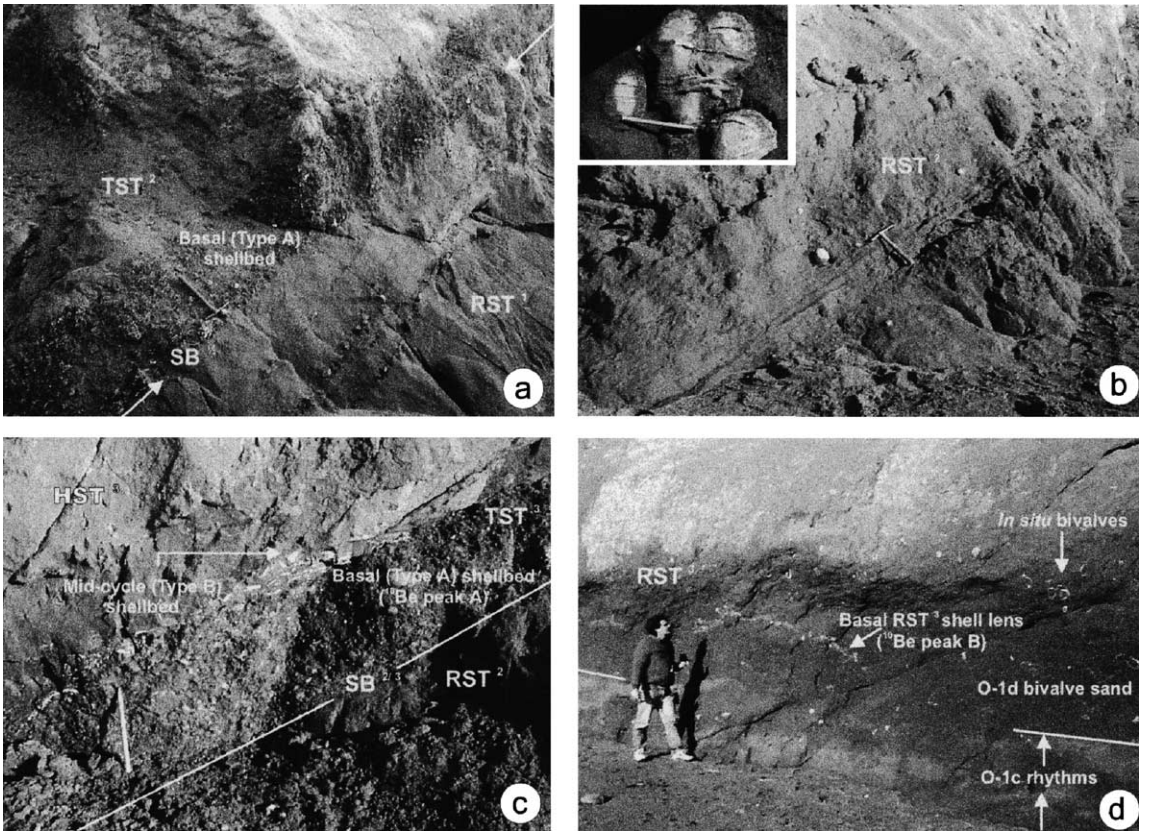

Fig. 4. Outcrop detail of sedimentary units within the Merced-2 and Merced-3 sequences. Hammer, where present, is 30 cm long. (a) Basal Type A shellbed and pebble layer of the Merced-2 Sequence, resting on an erosive surface on concretionary RST sands of the preceding cycle. (The apparent angular discrepancy across the sequence boundary is illusory, caused by foreshortening and changing angles of the main surface of outcrop.) (b) Concretionary bioturbated and bedded sands of the RST of the Merced-2 Sequence. Inset: cluster of *Scutellaster* from probable RST^3 shoreface sands (fallen block). (c) Basal compound shellbed, including a thin MCS, and overlying HST of the Merced-3 Sequence. Pencil gives scale. (d) Outcrop view of the HST^3–RST^3 transition, on the south side of Bivalve Point. Note the discontinuous, current-sorted shell-lens about 1 m above the O-1c/O-1d unit boundary. (e) Detail of the O-1c/O-1d unit boundary. Note the presence of carbonaceous fragments and residual lamination in the lower part of the O-1c rhythm, the "hummocky" top of the overlying and better cemented massive sand (light coloured), and the presence of in situ bivalved molluscs at the base of Unit O-1d. (f) Trough cross-bedded sands of Unit O-2, middle RST^3. (g) Unit O-2/O-3 boundary, with hammer resting on the coarser grained, laminated sand at the base of O-3. (h) Unit O-4/P-1 boundary, with hammerhead resting on a lens-shaped bar of cross-bedded granular sand.

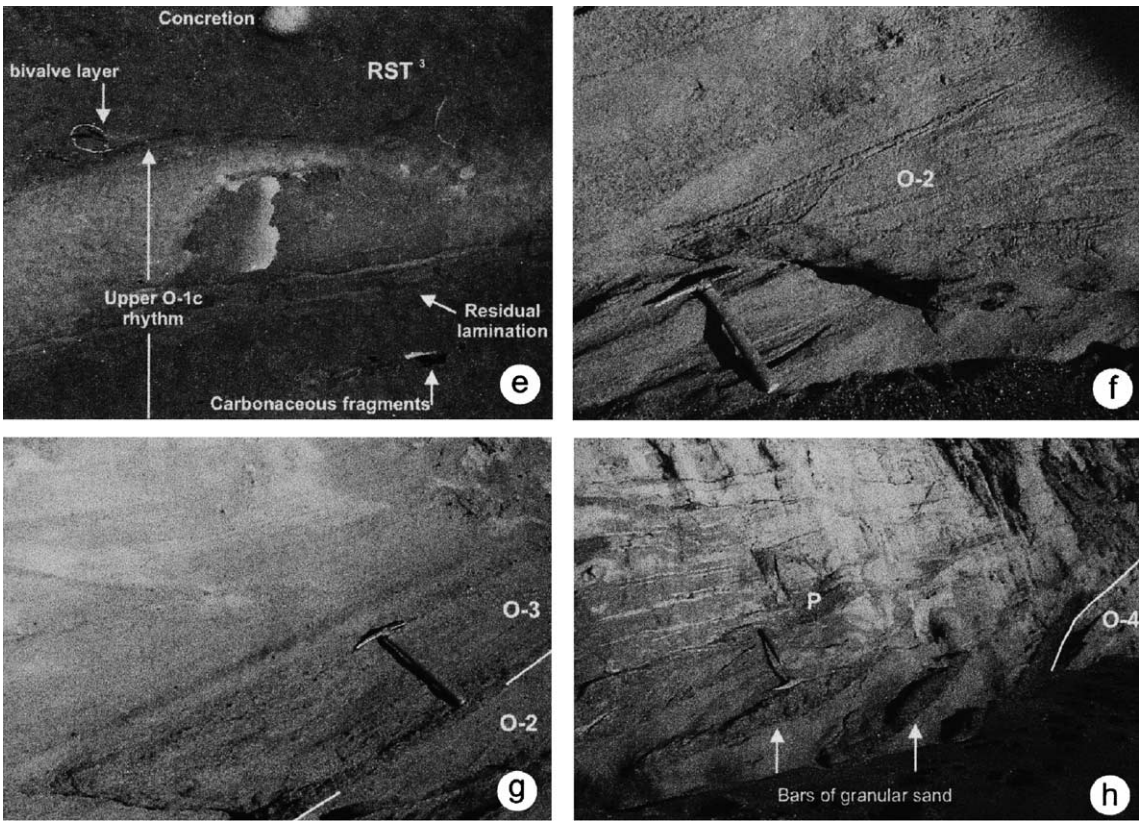

Fig. 4 (*continued*).

The top 3.5 m of the TST is equivalent to the lower part of unit N of Hunter et al. (1984), and comprises numerous thinner, rhythms that carry thin current-sorted shellbeds at their base. Our preferred interpretation is that these represent autocyclic fluctuations within the TST of the Merced-2 cycle.

Alternatively, it is possible that the lower N shellbeds (Fig. 2) represent either (i) shallow marine, perhaps even estuarine, shellbeds within an RST that extends upwards from unit M1; this would imply the relocation of the Merced-1/2 sequence boundary at +14.50 m, at the base of the presently labelled MCS; or (ii) transgressive Type A shellbeds at the base of a new cycle; in this case, the Merced-1/2 boundary would lie at +12 m, at the base of the shellbed package, and the M2–M3 sands would come to comprise a top-truncated sequence in their own right. The shallow water nature facies of Merced sediments, the abundant sediment supply and accommodation space that was available in the subsiding basin, and the tectonic overprint, make ambiguities of interpretation such as these inevitable. Though we have preferred to group the upper M–lower N succession together as the TST of our Merced-2 cycle, this does not preclude the existence of other plausible sequence interpretations of the same part of the succession.

2.2. Mid-cycle shellbed and highstand systems tract

A 30-cm-thick shellbed with in situ fossils in a fine sandy siltstone matrix (Type B shellbed of Abbott and Carter) occurs 14 m above the base of the Merced-2 cycle. Abrupt deepening occurs across this unit, which is interpreted as a mid-cycle shellbed, bounded by a local flooding surface below and a downlap surface above. The higher cliff-face above the shellbed is inaccessible, and at its top, the section abuts the fault (cf. Fig. 3a), but at least 6 m of massive, bioturbated grey sandy siltstone overlie the MCS, and comprise the highstand systems tract of cycle Merced-2.

2.3. Regressive systems tract

At beach level on the northern side of the fault occurs 4+ m of muddy sandstone that passes up into 8 m of massive fine sandstone encompassing a 20-cm-thick interval of parallel and ripple cross-bedded sandstone with abundant carbonaceous fragments (Figs. 2 and 4b). Scattered granules and rounded pebbles, shell fragments and carbonaceous fragments up to 3 cm in diameter occur scattered through the sandstone, together with tabular and ovoid carbonate concretions up to 20 cm in diameter, and rare in situ double-valved bivalves. Limonite-skeined microfaulting is widespread. We interpret this succession as the RST and top of the Merced-2 Sequence. However, and although we infer that the HST^2 siltstone on the south side of the fault originally graded up into the RST muddy sandstone and sandstone that is now easily accessible only on the north side of the fault, we are unable to prove stratigraphic continuity between our inferred HST^2 and RST^2 sediment bodies. It is therefore possible, though in our view unlikely, that one or more sequences have been cut out of the section by the fault, and that the two disjunct pieces of section that we have classified as TST^2–MCS^2–HST^2 and RST^2 actually belong to different sequences.

3. Sequence Merced-3

The Merced-3 cycle outcrops along the foot of the cliff around a small headland, here informally named "Bivalve Point", located about 150 m north of where the small fault that separates the main outcrops of the Merced-2 and Merced-3 sequences meets the beach (Fig. 3b,c). The entire Merced-3 Sequence is exposed around and north of Bivalve Point, though unit O-1a and the lower part of O-1b are frequently covered by slumps. Minor intra-sequence faulting is conspicuous throughout the section. The Merced-3 Sequence is exactly equivalent to units O–P1 of Hunter et al. (1984). The Beetle Bed at its top (unit P-2) marks LST^{nm4}, and also corresponds to the boundary between the Lower and Upper Members of the Merced Formation of Hall (1965); the accompanying switch of provenance from Franciscan to Great Valley-derived terrigenous detritus occurs in sand unit P1, a little below the Beetle Bed (Ed Clifton, pers. comm.). We recognize five subunits (Fig. 2), O-1a to O-1e, within unit O-1 of Hunter et al. (1984).

3.1. Transgressive systems tract and mid-cycle shellbed

The Merced-3 cycle commences with a sharp ravinement surface cut across RST concretionary sandstones of the underlying sequence, above which lies a 15-cm-thick pebbly shellbed (unit O-1a; Fig. 4c), similar to the basal bed of the Merced-2 Sequence. The O-1a shellbed is, however, compound (cf. Naish and Kamp, 1997; Kondo et al., 1998). The basal part (Type A shellbed) contains reworked single-valved molluscan shells and rounded quartz or lithic granules and pebbles up to 3 cm in diameter set in a poorly sorted sand matrix, and corresponds to a thin TST. The sediment is trimodal (Fig. 5). This is overlain by a 3-cm, sharp-based layer of mostly bed-parallel, double-valved bivalves and shell fragments in a matrix of muddy sand (Type B shellbed), which we interpret as the mid-cycle shellbed.

3.2. Highstand-regressive systems tract

As previously described by Hunter et al. (1984, p. 21), the section above the O-1a compound shellbed, corresponding to the bulk of their unit O, "comprises a complete progradational sequence from shelf to backshore". We agree with this interpretation, and infer that unit O represents the HST and lower RST of the Merced-3 Sequence. We also infer that unit P1 which lies above, and which was interpreted as a separate nearshore–foreshore cycle by Hunter et al. (1984), represents a paracycle within the upper RST of the same sequence.

The Merced-3 HST commences with massive, bioturbated, grey micaceous siltstone with scattered carbonaceous fragments, shell fragments and double-valved bivalves, some in life position (unit O-1b). A 5-cm-thick layer of bivalve shells, both single and double valved, and mostly layer parallel, occurs 1 m above the base, and may represent a downlap shellbed *sensu* Naish and Kamp (1997). Above this shell concentration, the HST^3 siltstone is cut by several sharp, low-angle shears, across which interval the sediment becomes coarser grained, and grades rapidly up into shoreface sands containing conspicuous large bivalve

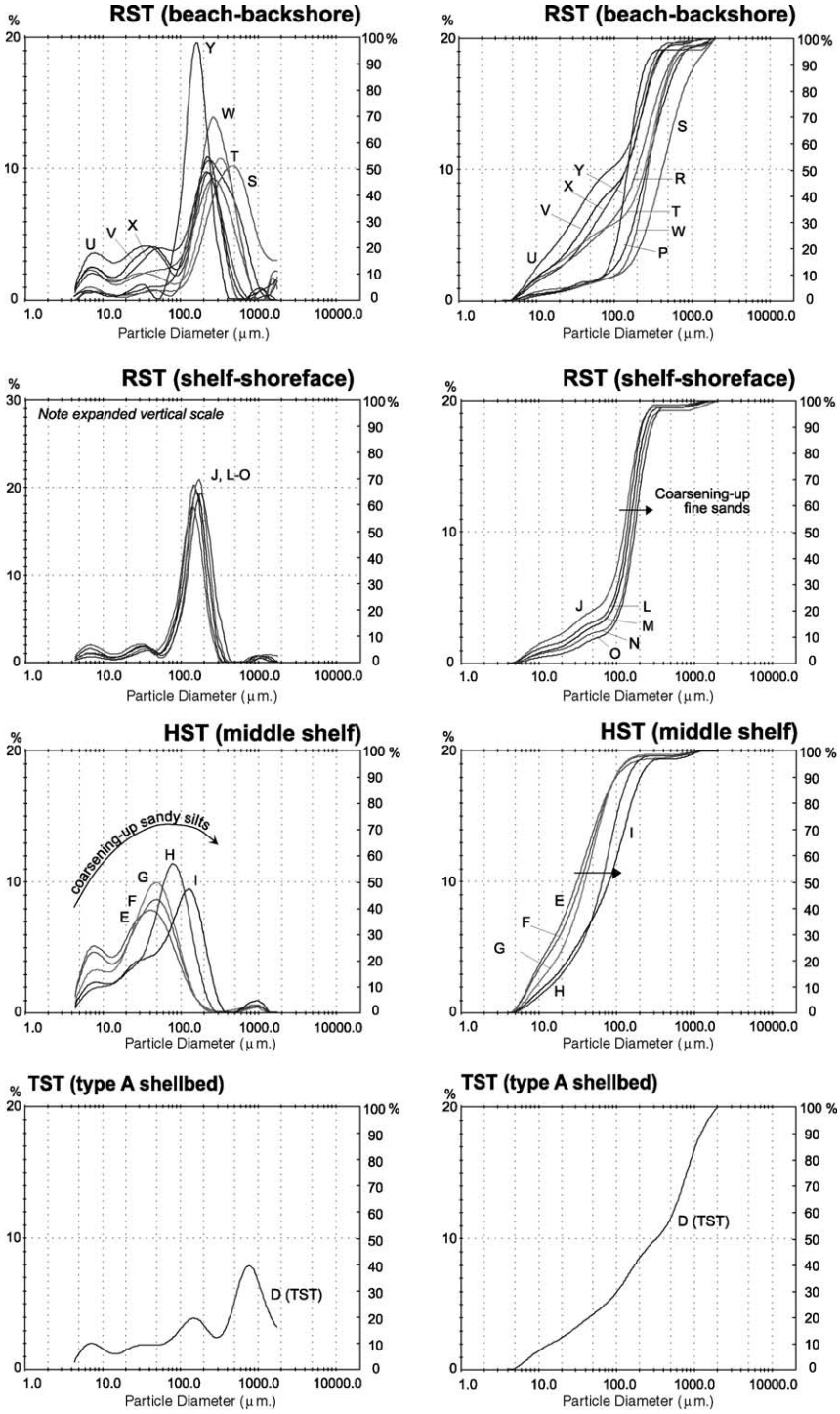
RST (beach-backshore)
RST (beach-backshore)
RST (shelf-shoreface)
Note expanded vertical scale
J, L-O
RST (shelf-shoreface)
Coarsening-up fine sands
HST (middle shelf)
coarsening-up sandy silts
HST (middle shelf)
TST (type A shellbed)
D (TST)
TST (type A shellbed)
D (TST)
Particle Diameter (μm.)
%

shells in life position (Fig. 3b). The O-1b siltstones become appreciably thicker (?less faulted) higher in the cliff. At the beach, they have a main mode that coarsens slightly from 40 μm at the base of the HST to 55 μm at the top (Fig. 5). They represent middle shelf mud-belt sediments that were probably deposited in water depths greater than c. 55 m (cf. Wright et al., 1999).

The transition between O-1b siltstones and O-1d shoreface sands (which we take to be the HST^3–RST^3 transition) is marked by two 50- to 60-cm-thick rhythms of bioturbated-to-massive sand overlain by a layer of bed-parallel shells, which all together comprise unit O-1c (Fig. 4d,e). The lower part of each rhythm comprises intensely bioturbated silty sandstone with scattered shells, wood fragments, and spherical concretions up to 5 cm in diameter, which passes rapidly up over a few millimeters into well-sorted, pervasively bioturbated, grey sandstone. (Hunter et al., 1984, p. 21, suggested that the barren sandstone intervals were "sheared" zones, perhaps implying an origin from liquefaction during earthquake activity.) The top of the bioturbated interval in the upper rhythm contains vestiges of current-lamination, and the overlying (upper) massive sand has a subplanar base and an undulating (perhaps hummocky) top, as a result of which the sand varies between c. 5 and 15 cm thick (Fig. 4e). Wright et al. (1999, p. 104) report a similar interbedding of current-rippled sands and bioturbated silts on the modern Eel River shelf at the junction of the inner shelf sand belt and the mid-shelf mud belt, at a depth of 55 m.

A bed-parallel interval of both single- and double-valved bivalves lies immediately above the sand of the upper rhythm, and passes upwards and laterally into a discontinuous current-sorted shellbed on some parts of the outcrop. The matrix to this shellbed comprises a slightly silty very fine sandstone with a main mode at 80 μm (Fig. 5, H). Samples taken across the O-1b to basal O-1d interval, that is, across the HST^3–RST^3 transition, display a subtle upward increase in the mean grain-size of the dominant very fine sand mode (Fig. 5). These various features are consistent with sediment deposition for unit O-1c in the zone of current and wave activity at the distal edge of the shore-connected sand prism, which marks also the sedimentary transition to the mid-shelf mud zone and lies at a depth of 50–60 m on the modern western USA shelf (e.g. Drake and Cacchione, 1985; Sommerfield and Nittrouer, 1999).

The interval of HST^3 shelf siltstone and transitional silty sandstone-rhythms is overlain by 9 m of RST^3 sandstone rich in mollusca, including large infaunal bivalves in life position (unit O-1d; Figs. 3b,c and 4d), and then by 8 m of unfossiliferous and mainly massive sandstone (unit O-1e). Though crude layering is apparent from a distance, the bedding detail in unit O-1d is largely disrupted by bioturbation, apart from a laterally discontinuous shell lens located about 1 m above the base (Fig. 4d), and a 15-cm-thick sharp-based interval of granular parallel-laminated sand and reworked convex-up bivalve shells located about 4 m above the base. The fauna is fragile and difficult to extract and identify, but surf zone and innermost shelf species are dominant, including *Trachycardium quadragenarium*, *Tresus nuttallii* and *Macoma* sp. The mollusc-rich sands are interpreted as shoreface surf zone deposits, and the thin shellbeds at the base and at 4 m probably represent storm lag deposits. The gradationally overlying 8 m of very well-sorted, unfossiliferous O-1e sandstone has between 17% and 21% of its volume present in the main (fine) sand mode, and displays a subtle but remarkably consistent coarsening in size of this mode from 150 to 190 μm with height gained in the section (Fig. 5). We therefore interpret the O-1d and O-1e sandstones as a continuously shoaling inner shelf to shoreface deposit.

Unit O-2, about 20 m above the base of the sequence, comprises a 4.5-m-thick interval of poorly sorted, low-angle planar bedded, or trough cross-bedded, granular, coarse to medium sandstones, with sharp bed bases (Fig. 4f), and was interpreted by Hunter et al. (1984, p. 21) as a nearshore facies. The overlying unit O-3 is a 3-m-thick interval of parallel-laminated tolow-angle cross-bedded very fine and fine sandstone with concentrations of mafic minerals (Fig. 4g), of probable foreshore origin (Hunter et al., 1984). The basal 35 cm

Fig. 5. Grain-size analyses of selected bulk samples through the Merced sequences. Left, modal histograms; right, cumulative frequency curves. From the base upwards, the sediment facies graphed are shellbed, highstand systems tracts silts, and regressive systems shelf-shoreface-beach sandstones. Letters D–Y refer to the sample localities shown in Fig. 2.

of O-3 comprises a graded granular coarse sand. Unit O-4 (Fig. 3c) is 7 m thick and comprises 20- to 40-cm-thick beds of bedded and laminated sand some of which contain climbing adhesion ripples indicative of subaerial exposure and probable backshore origin (Hunter et al., 1984, p. 21). The sediments represented by units O-2 to O-4 are mostly less well sorted than the O-1d to O-1e facies that they succeed. Though they often contain a sharp and dominant mode in the fine sand range of 230–280 μm, half of the O-2 to O-4 samples have bimodal silt tails (modes at c. 40 and <10 μm), and also often contain a significant component of very coarse sand (Fig. 5). These changes in sorting, and the associated sedimentary structures, support an interpretation of units O-1 to O-4 as a continuously shoaling "regressive" succession that passes up from inner shelf through beach to backshore deposits (cf. Hunter et al., 1984).

The contact between units O and P of Hunter et al. (1984) corresponds with the base of a series of sharp-based, lenticular, trough cross-bedded, 5- to 25-cm-thick, granular sands (Fig. 4h) that are interbedded with, and pass up into, better sorted cross-bedded and planar-bedded brown sandstones. The granular sand lenses are concentrated within the basal one-third of unit P, and have sharp, planar or slightly convex-downward bases, and sharp, curved, convex-upward tops, consistent with deposition as migrating gravel bars. The occurrence of rare shell fragments and the trace fossil *Macaronichnus* indicate a marine influence, and show that the base of unit P must be a local marine erosional (channel) or flooding surface. The upper parts of P-1 comprises massive or cross-bedded, well-sorted sand. The top c. 50 cm of P-1 has a leached appearance, displays rootlets, and represents a palaeosol below the 10- to 25-cm-thick P-2 lignite layer. Wing fragments of fossil beetles have been collected from the lignite that is hence termed the Beetle Bed (Hunter et al., 1984, p. 21).

We interpret unit P-1 as representing beach and probably estuarine sands deposited at the top of a shoreface, on the landward side of which occurred the protected, low-energy, coastal plain swamp that provided the plant material for the Beetle Bed. Unit P therefore represents the upper part of the RST of the Merced-3 Sequence (P-1), capped by the LST^{nm4} palaeosol and coastal swamp lignite (P-2) of the following glacial lowstand.

4. Beryllium isotope variation within the Merced-3 Sequence

The cosmogenic isotope ^{10}Be is produced in the upper atmosphere by spallation reactions between cosmic rays and oxygen or nitrogen. ^{10}Be is removed from the atmosphere mainly by rain, in attachment with aerosols, after which it enters soils, lakes or oceans either directly, or after aeolian and fluvial transport. With a relatively long half-life of 1.5 Ma, ^{10}Be occurs in all Plio-Pleistocene sedimentary deposits, with an abundance that varies according to age, latitude and the environment of deposition. Assuming (for a given latitude and age) a constant rate of atmospheric production for ^{10}Be, its abundance in seafloor sediments is closely related to its dilution amongst other components, that is, to the sedimentation rate, which for oceanic environments often varies in sympathy with climatic cycling (e.g. Eisenhauer et al., 1994).

Most previous sedimentary applications of ^{10}Be analysis have involved oceanic sediments. Recently, however, Graham et al. (1998) have demonstrated the isotope's usefulness as a palaeoenvironmental and stratigraphic indicator in studies of shallow marine, cyclothemic sediments from Wanganui Basin, New Zealand. That a recognisable and repetitive ^{10}Be pattern occurs in the cyclic Wanganui sediments has important implications. Possible explanations for ^{10}Be enrichment spikes include the melting of ice sheets, erosion of continental soils, enhanced biogenic scavenging, changes in sedimentation rate, and changes in the rate of atmospheric production caused by changes in the Earth's magnetic field or other global geophysical mechanisms. At Wanganui, however, ^{10}Be abundance has been shown to be closely related to the sequence stratigraphic architecture, and therefore also to sedimentation rate. Our measurements of ^{10}Be abundance in the Merced Formation were made to test the degree to which the pattern established at Wanganui might apply to all Pleistocene cyclothemic sequences.

In studying Be-isotope variation across the Merced-3 Sequence, we have followed the analytical procedures described by these authors and by Ditchburn et al. (1995), with the following exception. The two basal samples from sequence 3 were sieved to remove the >2-mm-size fraction (about 50% of the sample), which may have resulted in slightly enhanced ^{10}Be values for those samples.

In their study of mid-latitude, shallow-water, cyclothemic Pleistocene sediments from Wanganui, Graham et al. (1998) established that:

- transgressive shoreface sands (TST) and progradational shelf silts (HST) exhibit low values of ^{10}Be abundance, of the order of $0.5–1.0 \times 10^8$ atoms g^{-1}; these values represent the local background ^{10}Be level, and indicate a remarkably uniform rate of sedimentation, especially for the HST siltstones;
- within each cyclothem, significant ^{10}Be peaks of $2–6 \times 10^8$ atoms g^{-1} occur at the base of mid-cycle shellbeds (MCS), coincident with the local flooding surface (LFS), that is, a ^{10}Be peak corresponds precisely with the surface of inferred maximum sediment starvation within each cyclothem, and is estimated to represent a 2- to 4-ka hiatus in sedimentation; a steady decay of the LFS peaks occurs upwards through each MCS, with ^{10}Be values reaching the background level just above the contact with the overlying HST siltstone; and
- the ravinement surfaces that separate cylothems at Wanganui are in general not associated with ^{10}Be peaks; this is consistent with the inference, already established from sedimentological study, that marine erosion at the ravinement surfaces has removed any soil or non-marine sediment that formerly marked the underlying sequence boundary.

We have analysed for Be-isotopes through the Merced-3 Sequence (Figs. 2 and 6; Table 1). A systematic pattern of variation in ^{10}Be abundance occurs, but with peaks located at different levels to those established for the Wanganui cyclothems. We note the following characteristics of the ^{10}Be pattern across the Merced-3 Sequence:

- a level of 0.94×10^8 atoms g^{-1} of ^{10}Be characterizes the HST mid-shelf silts (unit O-1b), compared with the low background level of 0.22×10^8 atoms g^{-1} of ^{10}Be that characterizes upper shoreface sands in the same cycle (top of unit O-4);
- major ^{10}Be peaks occur near both the upper and lower sequence boundaries; peak A of 1.3×10^8 atoms g^{-1} of ^{10}Be is associated with the unit O-1a shellbed that rests on the basal ravinement surface/sequence boundary, and values up to 1.7×10^8 atoms g^{-1} of ^{10}Be characterize peak D that lies in the Beetle Bed lignite (unit P-2), at the upper sequence boundary;
- a slightly lower peak (B) of 1.1×10^8 atoms g^{-1} of ^{10}Be occurs near the HST/RST boundary, in the lagged shell lens that occurs just above the base of bivalve sand unit O-1d;
- the major (RST) part of the cycle is characterized by a gradual diminution of ^{10}Be values from those of the basal O-1d high to those at background level in upper unit O-4; minor steps occur in this diminution (i) at the top of the unit O-1d bivalve sand, and (ii) at the base of the P1 beach sand paracycle at the top of the Merced-3 Sequence.
- these major characteristics of ^{10}Be variation across the succession are mirrored by the ^{10}Be/^{9}Be curve, which is, however, smoother and has better defined peaks (Fig. 6). This is because the effects on ^{10}Be abundance of variations in grain size and carbonate content are largely eliminated by use of the ^{10}Be/^{9}Be ratio.
- significant variations also occur in the ^{9}Be plot, in particular the increase in ^{9}Be that occurs in the three samples from the Beetle Bed, and which may relate to an enhanced availability of ^{9}Be after the advanced chemical weathering caused by soil and lignite formation. Other increases in ^{9}Be appear unsystematic, for instance in unit O1b, an increase in ^{9}Be is associated with a decrease in ^{10}Be, whereas the converse is true for the sample from the base of unit P1.

It is evident from this pattern that, as already established for Wanganui cyclothems, the ^{10}Be signature of the Merced-3 Sequence reflects well the sequence stratigraphic architecture, and the absolute ^{10}Be values follow closely the cycle trends in sedimentary facies and grain size. Thus, ^{10}Be content may be used as a proxy for sediment accumulation rate (Graham et al., 1998). Consistent with this, ^{10}Be peaks are associated with shellbeds and lignites, both of which have slow sedimentation rates, whereas background ^{10}Be values characterize terrigenous shelf siltstones and shoreface sands.

^{10}Be peak A occurs within the Type A transgressive shellbed that marks the base of the Merced-3 Sequence (Fig. 4c). Similar transgressive shellbeds at Wanganui (the Kaikokopu and Kupe Formation shellbeds, Graham et al., 1998, Fig. 3) do not display ^{10}Be enrichment. We interpret this as indicating that the ^{10}Be enrichment in Merced unit O-1a results from the concentration within the shellbed of material eroded from the ^{10}Be-rich former top of underlying cycle N. This, together with (i) the very thin, reworked nature of unit O-1a, and (ii) the presence of inner shelf sand

Table 1
Be isotopic composition and carbonate contents of the Merced-3 Sequence

Sample no.	Height (m)	^{9}Be in dry sample (μg/g)	(1sd)	^{10}Be atoms/g	(1sd)	^{10}Be atoms/g CO_3 and decay corrected	(1sd)	Natural ^{10}Be/^{9}Be	(1sd)	^{10}Be/^{9}Be decay corrected	(1sd)
662	−0.4	0.256	0.006	4.22E+07	5.92E+06	6.11E+07	8.58E+06	2.46381E−09	3.51E−10	3.56551E−09	5.08E−10
663	−0.2	0.266	0.007	3.74E+07	1.20E+06	5.42E+07	1.74E+06	2.09924E−09	8.51E−11	3.03792E−09	1.23E−10
664	−0.05	0.285	0.007	4.02E+07	1.20E+06	5.82E+07	1.74E+06	2.10675E−09	8.14E−11	3.0488E−09	1.18E−10
665	0.01	0.247	0.006	8.46E+07	1.74E+06	1.23E+08	2.54E+06	5.12194E−09	1.67E−10	7.41224E−09	2.42E−10
666	0.1	0.255	0.007	8.54E+07	1.68E+06	1.31E+08	2.58E+06	5.00931E−09	1.61E−10	7.24926E−09	2.34E−10
667	0.14	0.335	0.008	8.28E+07	1.71E+06	1.22E+08	2.52E+06	3.69908E−09	1.15E−10	5.35315E−09	1.66E−10
668	0.2	0.382	0.009	8.93E+07	1.92E+06	1.31E+08	2.83E+06	3.49178E−09	1.09E−10	5.05315E−09	1.58E−10
669	0.35	0.399	0.009	8.10E+07	1.95E+06	1.17E+08	2.81E+06	3.03065E−09	1E−10	4.38582E−09	1.45E−10
678	0.45	0.428	0.010	8.28E+07	2.07E+06	1.28E+08	3.20E+06	2.89522E−09	9.68E−11	4.18984E−09	1.4E−10
679	0.95	0.328	0.008	6.91E+07	1.69E+06	1.03E+08	2.52E+06	3.14436E−09	1.07E−10	4.55037E−09	1.55E−10
680	1.15	0.407	0.010	8.48E+07	1.98E+06	1.31E+08	3.05E+06	3.1119E−09	1.01E−10	4.50341E−09	1.46E−10
681	2.15	0.400	0.009	6.20E+07	1.66E+06	9.39E+07	2.51E+06	2.31482E−09	8.1E−11	3.34991E−09	1.17E−10
682	2.55	0.411	0.010	6.23E+07	1.85E+06	9.40E+07	2.80E+06	2.26654E−09	8.47E−11	3.28003E−09	1.23E−10
683	3.15	0.340	0.008	5.81E+07	1.84E+06	8.56E+07	2.72E+06	2.55757E−09	1.01E−10	3.7012E−09	1.46E−10
684	3.25	0.348	0.008	7.41E+07	1.89E+06	1.12E+08	2.87E+06	3.18015E−09	1.1E−10	4.60218E−09	1.59E−10
685	3.35	0.327	0.008	6.86E+07	2.65E+06	1.04E+08	4.01E+06	3.14046E−09	1.43E−10	4.54473E−09	2.06E−10
686	3.95	0.309	0.008	7.40E+07	2.01E+06	1.11E+08	3.02E+06	3.58243E−09	1.3E−10	5.18434E−09	1.88E−10
687	4.35	0.298	0.008	6.37E+07	1.62E+06	9.68E+07	2.46E+06	3.18863E−09	1.12E−10	4.61444E−09	1.62E−10
688	5.15	0.280	0.007	5.30E+07	1.45E+06	8.03E+07	2.19E+06	2.82885E−09	1.04E−10	4.09378E−09	1.5E−10
689	8.35	0.266	0.007	4.98E+07	1.29E+06	7.45E+07	1.93E+06	2.80112E−09	1E−10	4.05366E−09	1.45E−10
690	9.65	0.267	0.007	4.59E+07	1.15E+06	6.80E+07	1.71E+06	2.56845E−09	9.17E−11	3.71694E−09	1.33E−10
694	11.65	0.248	0.007	3.29E+07	1.26E+06	4.83E+07	1.84E+06	1.98299E−09	9.18E−11	2.8697E−09	1.33E−10
692	14.25	0.234	0.006	3.14E+07	1.10E+06	4.59E+07	1.61E+06	2.00264E−09	8.89E−11	2.89813E−09	1.29E−10
693	16.85	0.245	0.006	3.16E+07	9.46E+05	4.61E+07	1.38E+06	1.92933E−09	7.6E−11	2.79204E−09	1.1E−10
695	19.45	0.154	0.005	1.68E+07	6.81E+05	2.45E+07	9.90E+05	1.63262E−09	8.58E−11	2.36265E−09	1.24E−10
696	23.25	0.169	0.005	1.60E+07	6.34E+05	2.30E+07	9.13E+05	1.41297E−09	7.16E−11	2.04479E−09	1.04E−10
698	25.75	0.278	0.007	2.44E+07	8.03E+05	3.58E+07	1.17E+06	1.31525E−09	5.44E−11	1.90338E−09	7.87E−11
697	28.45	0.243	0.006	1.95E+07	7.99E+05	2.84E+07	1.17E+06	1.19921E−09	5.86E−11	1.73544E−09	8.48E−11
699	32.85	0.252	0.007	1.54E+07	6.74E+05	2.23E+07	9.76E+05	9.11557E−10	4.65E−11	1.31916E−09	6.73E−11
700	33.25	0.225	0.006	1.81E+07	7.30E+05	2.62E+07	1.06E+06	1.20256E−09	5.87E−11	1.74029E−09	8.5E−11
701	33.4	0.174	0.005	2.55E+07	7.94E+05	3.68E+07	1.15E+06	2.19137E−09	9.47E−11	3.17125E−09	1.37E−10
702	38.3	0.154	0.005	1.23E+07	5.75E+05	1.79E+07	8.34E+05	1.19608E−09	6.97E−11	1.73092E−09	1.01E−10
703	41.9	0.176	0.006	1.01E+07	5.23E+05	1.47E+07	7.59E+05	8.56249E−10	5.2E−11	1.23913E−09	7.52E−11
704	42.05	0.127	0.005	6.06E+06	4.19E+05	8.85E+06	6.12E+05	7.13004E−10	5.65E−11	1.03183E−09	8.18E−11
705	42.25	0.123	0.005	5.89E+06	3.88E+05	8.55E+06	5.64E+05	7.14261E−10	5.5E−11	1.03365E−09	7.96E−11
706	42.35	0.271	0.007	4.82E+07	1.14E+06	7.17E+07	1.70E+06	2.6572E−09	9.13E−11	3.84539E−09	1.32E−10
707	42.4	0.243	0.007	4.90E+07	1.17E+06	7.36E+07	1.76E+06	3.01665E−09	1.08E−10	4.36556E−09	1.57E−10
708	42.45	0.279	0.008	1.08E+08	1.93E+06	1.71E+08	3.05E+06	5.79353E−09	1.79E−10	8.38414E−09	2.6E−10

Note that all ^{10}Be concentrations are corrected for age = 800 ka and carbonate content, and expressed in terms of the total dry sample. Carbonate percentage is calculated from weight loss during acid dissolution. All errors, 1 sigma.

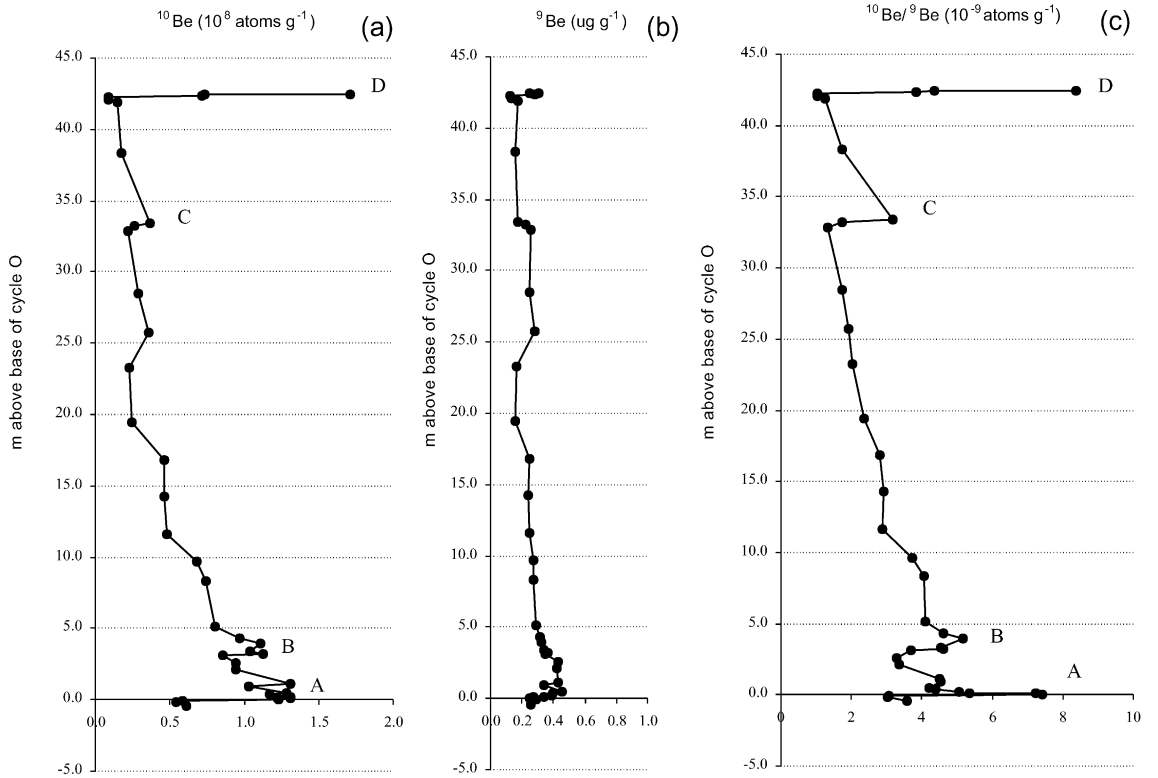

Fig. 6. Be-isotope concentration profile across the Merced-3 Sequence. (a) ^{10}Be concentration, (b) ^{9}Be concentration, (c) ^{10}Be/^{9}Be ratio. The ^{10}Be concentration is age corrected, and expressed as atoms g^{-1} dry bulk sediment.

at the top of unit N (Hunter et al., 1984, p. 21), suggests that less material has been eroded from the top of the Merced-2 cycle than what occurs across similar boundaries at Wanganui. Above peak A, ^{10}Be values decline gradually to those of the HST shelf siltstone background. This decline in ^{10}Be values is consistent with a gradual increase in the mid-shelf mud sedimentation rate through the HST, thin though the HST is in this cycle. A single anomalously high ^{10}Be value associated with a shell-rich lens 1.05 m above the base of unit O-1b is not accompanied by a high ^{10}Be/^{9}Be ratio (which is the same as that of the preceding sample); this peak may therefore be erroneous.

^{10}Be peak B occurs at the laterally discontinuous shell lens located just above the base of unit O-1d (Fig. 4d). The bed contains transported and mainly single-valved shells, and probably represents a wave-base shell-lag concentration. It is clear from the enclosing stratigraphy that this shell lens is not a mid-cycle shellbed *sensu* Abbott and Carter (1994). That the bed is nonetheless associated with a prominent ^{10}Be peak shows that, like MCSs, it does represent relative sediment starvation, doubtless a result of bypassing of finer grained sediment offshore after wave-induced suspension. (It is noteworthy that a higher shellbed, located near the middle of unit O-1d, is not accompanied by a ^{10}Be peak, which implies that the production of enhanced Be-values requires a concentration process over and above that which leads to the production of minor, autocyclic, shell layers and lags.) Above peak B, ^{10}Be values decline systematically across units O-1d through O-4. The shape of the declining curve indicates (i) that the unit O-1d bivalve sand, which is inferred to be a surf-zone deposit, accumulated more slowly (i.e. was subjected to more sediment bypassing) than the beach sand units that lie above it; (ii) that a surprisingly regular, gradual increase in net sedimentation rates accompanied the

deposition of the prograding RST shoreface represented by units O-1e to O-4; and (iii) that a sharp basal increase of ^{10}Be (peak C) followed by a decline to background values marks the unit P-1 beach sand, which therefore corresponds to a minor depositional paracycle within the top part of the Merced-3 Sequence.

^{10}Be peak D is defined by three samples with sharply increasing values that are located at the very top of the Merced-3 Sequence, within the Beetle Bed lignite. The Merced-3/Merced-4 sequence boundary is here marked by unconsolidated beach sand of cycle Q that rests directly on the Beetle Bed. Thus, and unusually for most of the Plio-Pleistocene sequences described to date (cf. Abbott, 1992), the Beetle Bed represents the preservation at the sequence boundary of sediments that accumulated during a glacial LST^{nm} environment. Not surprisingly, given that ^{10}Be is known to concentrate at the land surface and in soils (e.g. Barg et al., 1997), a high concentration of ^{10}Be occurs, with a peak just below the sequence boundary that reaches about 20 times the background level that characterizes the underlying, near-contemporaneous shoreface sand.

In summary, the ^{10}Be profile across the Merced-3 Sequence (Fig. 6) demonstrates the presence of significant ^{10}Be peaks associated with both the lower and upper sequence boundaries. The lower peak (A) is assumed to be reworked, because it corresponds to high values within the transgressive Type A shellbed that marks the base of the cycle. The upper peak (D) marks lignite accumulation, and ^{10}Be concentration, within a glacial coastal plain swamp. Between these peaks, a further ^{10}Be concentration (peak B) occurs within a shellbed near the base of the RST, and is inferred to have been caused by wave-suspension bypassing. ^{10}Be values throughout the rest of the Merced-3 Sequence exhibit three trends of gradual decline, one within HST shelf silts and two within RST shoreface sands, each of which is inferred to represent a subcycle of increasing sedimentation rate.

5. Discussion of sequence stratigraphic significance

The shallow water sedimentary cycles preserved within the Merced Formation are typical of deposits laid down under the influence of the high-frequency glacio-eustatic sea-level changes of the Plio-Pleistocene (Clifton, 1988; Clifton et al., 1988). Each cycle represents a stratigraphic sequence if it can be shown to be bounded below and above by unconformities that correspond to sea-level withdrawal during the preceding and ensuing glacial periods. Though Clifton (1989) noted the rarity of unequivocal sequence boundaries of this type within the Merced Formation, we suggest that such boundaries can be inferred within the Merced-1 to Merced-3 part of the succession. Within the sequences thus defined, characteristic sedimentary lithofacies succeed one another in a predictable order, and can be grouped into genetic systems tracts (Payton, 1977). In general, Plio-Pleistocene shallow marine sequences comprise, in ascending order, a transgressive systems tract, a mid-cycle shellbed, a highstand systems tract, and sometimes a regressive systems tract (Abbott and Carter, 1994; Naish and Kamp, 1997).

We interpret the basal surfaces of the Merced-2 and Merced-3 sequences as marine ravinement surfaces that have been superposed upon the original sequence boundaries during post-glacial shoreline transgression. In contrast, an in situ sequence boundary is represented by the LST^{nm4} Beetle Bed and its subjacent palaeosol, which is preserved at the top of the Merced-3 cycle.

The basal shellbed of Merced-2, and the lower part of the basal shellbed from Merced-3, are similar to the Type A shellbeds described by Abbott and Carter (1994) from the TSTs of New Zealand Pleistocene cyclothems. Similar shellbeds from late Pliocene sequences in the Rangitikei Valley were termed onlap shellbeds by Naish and Kamp (1997), and represent transgressive lag deposits formed by shoreface erosion and cannibalisation during rapid marine transgression (Abbott, 1998). The overlying well-sorted sands of the lower part of the Merced-2 cycle are of shoreface origin, and comprise the TST.

The Type B shellbeds that mark the middle of both the Merced-2 and Merced-3 cycles are bounded by inferred local flooding surfaces below and downlap surfaces above, and correspond to the mid-cycle shellbeds (MCS) described from New Zealand (Abbott and Carter, 1994; Abbott, 1997). A MCS is the sedimentary pivot around which a typical inner shelf glacio-eustatic cyclothem is organised; transgressive sediments deposited during a rising sea level lie below, and highstand and regressive sediments, deposited mostly during a static or falling sea level, lie above. After the landward

movement of the shore-connected sedimentary prism that is manifested by the local flooding surface, sediment starvation occurs on the middle shelf and beyond. In such a setting, in situ or near situ shellbeds develop, which are dominated by shellground taxa but which also have an accompanying infauna living in patches of soft-bottom between areas of shell accumulation (Abbott and Carter, 1997). Such shellbeds have been interpreted as backlap shellbeds by Naish and Kamp (1997).

In keeping with this interpretation, in the Merced-3 Sequence, the deepest water siltstones (O-1b) occur immediately above the MCS, and are followed by an almost 40-m-thick, continuously shoaling, regressive sedimentary sequence (RST). As described earlier by Hunter et al. (1984), all the major environments that characterize the modern Californian inner shelf and shoreface are superposed in the Merced-3 cycle in vertical Waltherian order (Fig. 2): coarsening upward, middle shelf siltstones (O-1b to O-1c); a thin zone of wave-base winnowed sediment (basal O-1d shell lens); a zone of sandstone with in situ bivalved clams (O-1d; surf zone shoreface); a unit of coarsening upward, very well-sorted massive sandstones (O-1e; lower beach); low-angle planar cross-bedded or trough cross-bedded, coarse to medium sandstone (O-2; middle–upper beach); laminated fine sand with mafic mineral concentrations along low-angle, tabular cross-sets (O-3; upper beach); rhythmic, slightly silty sandstones with climbing adhesion ripple marks (O-4; upper beach to backshore); cross-bedded beach sand with bars of granular sand (P1; estuarine flats and beach); and a palaeosol capped by thin lignite (Beetle Bed; coastal swamp).

The development of such a thick, continuously regressive, sedimentary cycle requires the presence of a substantial terrigenous sediment supply, and a static or falling sea level. Naish and Kamp (1997) have shown that the upper sandy parts of similar thick, continuously regressive sequences from New Zealand late Pliocene cyclothems were probably deposited during post-highstand sea-level fall, and comprise regressive systems tracts (RST). By analogy, we infer that the upper part of the Merced-2 and Merced-3 cycles, and of the other similar Merced cycles described by Hunter et al. (1984), represent RSTs. In any particular cycle, the boundary between the HST and RST is arbitrary and generally gradational. For the Merced-3 Sequence, we judge that it is best corresponds to unit O-1c, which marks the transition between mainly aggradational shelf siltstones below (O-1b) and the progradational, sandy, shoreface sands above (O-1d and higher units). As reported also by Naish and Kamp (1997) for many New Zealand RSTs, and given the high sediment supply that characterises the Merced cycles, there is no necessary "regressive surface of erosion" at the base of individual RSTs.

The emplacement at the top of the Merced-3 Sequence of the unit P-1 beach sand with an erosive base and basal gravel bars, followed by development on top of the beach of a palaeosol and lignite, marks a final marine influence that was followed by subaerial erosion and the development of non-marine coastal plain sedimentation. Unit P was interpreted as a thin but full cycle in its own right by Hunter et al. (1984). Though such an interpretation may be correct, given that the typical thickness of a Merced cyclothem is several tens of metres, we prefer to treat unit P as a final sedimentary pulse, or paracycle, within the Merced-3 cycle.

Sequence motifs similar to those we have described from the Merced Formation are also known from the Plio-Pleistocene of New Zealand. In particular, the Merced-2 Sequence, with its well-sorted TST sands, and probably continuous HST–RST, is similar to the *Seafield Motif cyclothem* of Saul et al. (1999; note, however, that any RST sands have been eroded from the top of the type example of the Seafield Motif). The Merced-3 Sequence, with a basal compound shellbed in which the TST is represented only by a thin, reworked shell and pebble layer, and with a thick and continuous HST–RST, is similar to the *Rangitikei Motif cyclothem* described by Naish and Kamp (1997).

Continental shelf sequences similar to those of the Merced Formation are now known from New Zealand (Fleming, 1953; Vella, 1963; Abbott et al., 1989; Abbott and Carter, 1994), Japan (Tokuhashi and Kondo, 1989; Kitamura and Kondo, 1990; Ito, 1992), Italy (Rio et al., 1996), and most recently Taiwan (Chen et al., 2001). Many of these authors have also shown that sequences deposited landward of the lowstand shoreline each correspond to an interglacial (odd-numbered) oxygen isotope stage. Studies of such Plio-Pleistocene glacio-eustatic sequences have the potential to contribute greatly to our understanding of how sedimentary sequences are deposited in general (e.g. Carter et al., 1998).

6. Conclusions

The exposure above sea level of a thick sequence of middle Pleistocene marine sediments is unusual, in that it requires a tectonic subsidence–uplift cycle on a scale of hundreds of metres within a time scale of only a few hundred thousand years (Saul et al., 1999). Such conditions are generally restricted to plate boundary areas, which is why the best known examples of Plio-Pleistocene sequence stratigraphy come from Japan and New Zealand. The sedimentary and tectonic cycles in each case are those of a consuming plate margin, in both forearc and backarc settings. The Merced Formation is located in a different tectonic setting, that of a conservative, transform-fault margin. The Merced Formation is important both for that reason, and also because it provides a rare onland example in North America of thick, cyclic, marine Pleistocene sediment. Studies of ^{10}Be concentration within the Merced-3 Sequence, and in similar cyclothems from New Zealand, show that the abundance of ^{10}Be is an accurate indicator of sequence stratigraphic architecture, and that it varies closely in sympathy with changes in inferred sedimentation rate.

Acknowledgements

Financial support for this research was provided by the Australian Research Council. We thank Alan Beu for his help with fossil identification, Bob Ditchburn and Albert Zondervan for performing the ^{10}Be analyses, Ed Clifton and Al Hine for their critical comments on the draft manuscript, and Helen and Bill Lindqvist for their warm hospitality. We particularly appreciate the kindness shown to us by Ralph Hunter, who introduced RMC to the Merced section in the field in 1994, and Ed Clifton, who generously provided a copy of his unpublished detailed measured section of the units M–P part of the succession, and showed great patience in suggesting many improvements to successive manuscript drafts.

References

Abbott, S.T., 1992. The mid-Pleistocene Waiomio Shellbed (c. 500–600 ky), Wanganui Basin, New Zealand. Alcheringa 16, 171–180.

Abbott, S.T., 1997. Mid-cycle condensed shellbeds from mid-Pleistocene cyclothems, New Zealand: implications for sequence architecture. Sedimentology 44, 805–824.

Abbott, S.T., 1998. Transgressive systems tracts and onlap shellbeds from mid-Pleistocene sequences, Wanganui Basin, New Zealand. J. Sediment. Res. 68, 253–268.

Abbott, S.T., Carter, R.M., 1994. The sequence architecture of mid-Pleistocene (0.35–0.95 Ma) cyclothems from New Zealand: facies development during a period of known orbital control on sea-level cyclicity. In: de Boer, P.L., Smith, D.G. (Eds.), Orbital Forcing and Cyclic Sequences, Int. Assoc. Sedimentol., Spec. Publ., vol. 19. Blackwell Scientific, Oxford, pp. 367–394.

Abbott, S.T., Carter, R.M., 1997. Macrofossil associations from mid-Pleistocene cyclothems, Castlecliff section, New Zealand: implications for sequence stratigraphy. Palaios 12, 182–210.

Abbott, S.T., Haywick, D.W., Carter, R.M., Henderson, R.A., 1989. Facies signature of late Neogene eustatic sea-level fluctuations exemplified in Plio-Pleistocene cyclothems, North Island, New Zealand. 28th Int. Geol. Cong., Washington (D.C.), Abstr., pp. 1–2.

Barg, E., Lal, D., Pavick, M.J., Caffee, M.W., Southon, J.R., 1997. Beryllium geochemistry in soils: evaluation of ^{10}Be/^{9}Be ratios in authigenic minerals as a basis for age models. Chem. Geol. 140, 237–258.

Carter, R.M., 1998. Two models: global sea-level change and sequence stratigraphic architecture. Sediment. Geol. 122, 23–36.

Carter, R.M., Naish, T.R., Ito, M., Pillans, B.J. (Eds.), 1998. Sequence stratigraphy in the Plio-Pleistocene: an evaluation. Sediment. Geol., Spec. Issue, vol. 122. Elsevier, Amsterdam, pp. 1–284.

Chen, W.-S., Ridgway, K.D., Horng, C.-S., Chen, Y.-G., Shea, K.-S., Yeh, M.-G., 2001. Stratigraphic architecture, magnetostratigraphy, and incised-valley systems of Pliocene–Pleistocene collisional marine foreland basin of Taiwan. Geol. Soc. Am. Bull. 113, 1249–1271.

Chiocci, F.L., Clifton, H.E., 1991. Gravel-filled gutter casts in nearshore facies—indicators of ancient shoreline trend. Soc. Econ. Paleontol. Mineral., Spec. Publ. 46, 76.

Clifton, H.E., 1988. Sedimentologic approaches to paleobathymetry, with applications to the Merced Formation of central California. Palaios 3, 507–522.

Clifton, H.E., 1989. Stratigraphic sequence response to glacioeustatic fluctuations in a rapidly subsiding Cenozoic basin, San Francisco, California. In: Morton, R.A., Nummedal, D. (Eds.), Gulf Coast Section, SEPM Foundation Seventh Annual Research Proceedings, pp. 203–211.

Clifton, H.E., Leithold, E.L., 1991. Quaternary coastal and shallow marine facies sequences, northern California and the Pacific Northwest. In: Morrison, R.B. (Ed.), Quaternary Nonglacial Geology, Conterminous United States, Geological Society of America, DNAG v. K-2, pp. 1156–1453.

Clifton, H.E., Hunter, R.E., Gardner, J.V., 1988. Analysis of eustatic, tectonic and sedimentologic influences on transgressive and regressive cycles in the Upper Cenozoic Merced Formation, San Francisco, California. In: Kleinspehn, K.L., Paola, C. (Eds.), New Perspectives in Basin Analysis. Springer-Verlag, New York, pp. 109–128.

Ditchburn, G.D., Graham, I.J., Sparks, R.J, Whitehead, N.E., 1995. Analytical methods for measuring ^{10}Be in marine sediments. Institute of Geological and Nuclear Sciences (Lower Hutt, New Zealand), Sci. Rep. 95/31, pp. 1–11.

Drake, D.E., Cacchione, D.A., 1985. Seasonal variation in sediment transport on the Russian River shelf. Cont. Shelf Res. 4, 495–514.

Eisenhauer, A., Spielhagen, R.F., Frank, M., Hentzschel, G., Mangini, A., Kubik, P.W., Dittrich-Hannen, B., Billen, T., 1994. ^{10}Be records of sediment cores from high northern latitudes: implications for environmental and climatic changes. Earth Planet. Sci. Lett. 124, 171–184.

Fleming, C.A., 1953. The geology of the Wanganui Subdivision, Waverley and Wanganui sheet districts (N137 and N138). N. Z. Geol. Surv. Bull. 52, 1–362.

Graham, I.J., Ditchburn, R.G., Whitehead, N.E., 1998. ^{10}Be spikes in Plio-Pleistocene cyclothems, Wanganui Basin, New Zealand: identification of the local flooding surface (LFS). Sediment. Geol. 22, 193–215.

Hall, N.T., 1965. Petrology of the type Merced Group, San Francisco Peninsula, California. Unpublished MA thesis, University of California, Berkeley, pp. 1–126.

Hunter, R.E., Clifton, H.E., Hall, N.T., Csaszar, G., Richmond, B.M., Chin, J.L., 1984. Pliocene and Pleistocene coastal and shelf deposits of the Merced Formation and associated beds, northwestern San Francisco Peninsula, California. Soc. Econ. Paleontol. Mineral., Field Guidebook 3, 1–29 (Mid-year meeting, San Jose).

Ito, M., 1992. High-frequency depositional sequences of the upper part of the Kazusa Group, a middle Pleistocene forearc basin fill in Boso Peninsula, Japan. Sediment. Geol. 76, 155–175.

Kitamura, M., Kondo, Y., 1990. Cyclic change of sediments and molluscan fossil associations caused by glacio-eustatic sea-level changes during the early Pleistocene—a case study of the middle part of the Omma Formation at the type locality. J. Geol. Soc. Jpn. 96, 19–36 (English abstract).

Kondo, Y., Abbott, S.T., Kitamura, A., Kamp, P.J.J., Naish, T.R., Kamataki, T., Saul, G.S., 1998. The relationship between shellbed type and sequence architecture: examples from Japan and New Zealand. Sediment. Geol. 122, 109–127.

Lanphere, M.A., Champion, D.E., Clynne, M.A., Muffler, L.J.P., 1999. Revised age of the Rockland tephra, northern California: implications for climate and stratigraphic reconstructions in the western United States. Geology 27, 135–138.

Lanphere, M.A., Champion, D.E., Clynne, M.A., Muffler, L.J.P., 2000. Revised age of the Rockland tephra, northern California: implications for climate and stratigraphic reconstructions in the western United States: reply. Geology 28, 287.

Larcombe, P., Carter, R.M., 1998. Sequence architecture during the Holocene transgression: an example from the Great Barrier Reef shelf, Australia. Sediment. Geol. 117, 97–121.

Meyer, C.E., Sarna-Wojcicki, A.M., Hillhouse, J.W., Woodward, M.J., Slate, J.L., Sorg, D.H., 1991. Fission-track age (400,000 yr) of the Rockland tephra, based on inclusion of zircon grains lacking fossil fission tracks. Quat. Res. 35, 367–382.

Naish, T.R., Kamp, P.J.J., 1997. Pliocene–Pleistocene shelf cyclothems from Wanganui Basin, New Zealand: high resolution facies and sequence stratigraphic analysis. Geol. Soc. Am. Bull. 109, 978–999.

Payton, C.E. (Ed.), 1977. Seismic stratigraphy—applications to hydrocarbon exploration. Am. Assoc. Pet. Geol. Mem., vol. 26, pp. 1–516.

Rio, D., Channell, J.E.T., Massarei, F., Poli, M.S., Sgavetti, M., D'Alessandro, A., Prosser, G., 1996. Reading Pleistocene eustasy in a tectonically active shelf setting (Crotone Peninsula, southern Italy). Geology 24, 743–746.

Sarna-Wojcicki, A.M., Meyer, C.E., Bowman, H.R., Hall, N.T., Russell, P.C., Woodward, M.J., Slate, J.L., 1985. Correlation of the Rockland ash bed, a 40,000-year-old stratigraphic marker in northern California and western Nevada, and implications for middle Pleistocene paleogeography of central California. Quat. Geol. 23, 236–257.

Saul, G., Naish, T.R., Abbott, S.T., Carter, R.M., 1999. Sedimentary cyclicity in the marine Plio-Pleistocene: sequence stratigraphic motifs characteristic of the last 2.5 Ma. Geol. Soc. Am. Bull. 111, 524–537.

Sommerfield, C.K., Nittrouer, C.A., 1999. Modern accumulation rates and a sediment budget for the Eel shelf: a flood-dominated depositional environment. Mar. Geol. 154, 227–241.

Tokuhashi, S., Kondo, Y., 1989. Sedimentary cycles and environments in the middle–late Pleistocene Shimosa Group, Boso Peninsula, central Japan. J. Geol. Soc. Jpn. 95, 933–951.

Vella, P., 1963. Pliocene–Pleistocene cyclothems, Wairarapa, New Zealand. Trans. R. N. Z., Geol. 2, 15–50.

Wright, L.D., Kim, S.-C., Friedrichs, C.T., 1999. Across-shelf variations in bed roughness, bed stress and sediment suspension on the northern California shelf. Mar. Geol. 154, 99–115.